Desalination and Water Treatment
www.deswater.com

doi: 10.5004/dwt.2019.24644

167 (2019) 218–230
November

Removal of nitrate from water by modified nano-clay and comparison with nano-graphene, nano-Fe_3O_4 and nano-clay – isotherm and kinetic studies

Hassan Masoudi, Fateme Ravari*, Hamid Mosaddeghi

Department of Chemistry, Payame Noor University, Tehran, P.O. Box: 3697-19395, Iran, Tel. +989399299136;
emails: hassan_masoudi2000@yahoo.com (H. Masoudi), fatemeravari@yahoo.com (F. Ravari), h.mosaddeghi@gmail.com (H. Mosaddeghi)

Received 27 January 2019; Accepted 1 July 2019

ABSTRACT

Application of diverse adsorbents (graphene, nano-Fe_3O_4, nano-clay and organically modified nano-clay [ONC]) in adsorbing nitrate from aqueous solution has been studied. Four adsorption isotherm models (Langmuir, Freundlich, Temkin, and Dubinin–Radushkevich) were applied to fit the adsorption data at equilibrium and the optimal isotherm of each adsorbent was found. Furthermore, three kinetic models (pseudo-first-order, pseudo-second-order, and intra-particle diffusion) were performed to fit the adsorption data for all of the above-mentioned adsorbents. The highest adsorbent capacity (q_m) enhances from 44.64 to 243.90 mg g^{-1} with changing adsorbent from graphene to modified nano-clay. The sequence corresponding to q_m obtained to be as the subsequent by altering the adsorbents: graphene < nano-Fe_3O_4 < nano-clay < ONC. Comparison of the correlation coefficients corresponding to adsorption isotherms shows that fitting graphene is better than the Dubinin–Radushkevich model, however, three other adsorption procedures fit with the Langmuir model. The adsorption kinetics is studied through fitting the observed time profiles into the pseudo-first-order (PFO), pseudo-second-order, and intra-particle diffusion (IPD) kinetic models. Adsorbing nitrate by graphene, coordinates well with the pseudo-second-order model and also with IPD model with two separated straight lines representing that two phases affect the sorption procedure. Nano-Fe_3O_4 adsorption procedure follows both first-order and second-order models. The IPD model is completely in agreement with the adsorption by nano-clay with a straight line, representing that the sorption procedure is controlled with intra-particle diffusion. Both pseudo-second-order model and IPD model can be utilized for describing the sorption kinetics by ONC. Based on the PFO model and comparison of kinetic constant (k_1), the order of adsorption speed was graphene < nano-Fe_3O_4 < nano-clay < ONC.

Keywords: Adsorption; Nitrate; Isotherm; Kinetics

1. Introduction

Nitrate and nitrite are usual contaminants in the polluted surface or groundwater and wastewater. The wastewater corresponding to the industrial fabrication procedure must be treated to recycle water as much as conceivable. Protecting water resources and extensive water management are essential because of the water shortage. By the way, the elimination of pollutants from water due to human activities or natural phenomena including nitrogen cycle is unavoidable. Dangerous impacts of nitrate ion on the human health (methemoglobinemia and other illnesses), and the ecosystem (eutrophication phenomena) [1], its impact on infants (blue-baby syndrome) [2], and several studies that reported the application of drinking water comprising high concentrations of NO_3^- could cause certain illnesses including central nervous system difficulties, birth defects, and stomach cancer [3,4], are pieces of evidence that removing nitrate and nitrite from drinking water is essential for preventing the dangerous impacts on human health. The nitrate

* Corresponding author.

concentration limit in drinking water in Iran is 50 mg $L^{-1,}$ which is as the same as in several countries in Europe. The World Health Organization (WHO) has considered the highest limit of nitrate to 50 mg L^{-1} in drinking water. Removing nitrate can be carried out by chemical [5], physical (reverse osmosis or electrodialysis) [6,7], physical–chemical (ion exchange) [8] or biological approaches [9]. Moreover, organic carbon resources may be used as electron donors for heterotrophic denitrification [10], which is valuable in biological treatment. Adsorption is more suitable for removing metal ions as it is a green and cost-effective technique and results in solid and reusable adsorbent [11]. Mineral clays could adsorb a wide range of heavy metal ions because of their reactive surface features, high specific surface area (SSA), and excellent cationic exchange capacities [12–14]. Titana pillared clays are reported for adsorption enhancement and photo-catalytic oxidation of methylene blue [15]. Excellent water absorption is the key disadvantage for montmorillonite clay associating with the problems of separation of ions. The surface features of clay minerals are considerably progressed (intercalation) by replacing interlayer cations of mineral clays with organic cationic surfactants [16]. Modification of clays with positively charged natural amino acids by intercalation in aqueous solution leads to organophile, biocompatible and biodegradable compounds [17–19]. Organic surfactants are usually applied to create clay's surface organophilic and swell the clay galleries [20,21]. These organically modified nano-clays (ONC) have many applications in different areas, including adsorbents for organic contaminants, metal ions, and catalysts [14,22,23]. Several properties of organically modified nano clays, such as their excellent specific surface, nano-scale, and the great tendency for adsorbing ions and organic compounds, led them to be used appropriately as an adsorbent for removing organic and inorganic contaminants. Additionally, other attractive aspects of ONC, including non-toxicity, excellent hydrophobicity, high biocompatibility, cost-effective, and reusability, provide its application for removing contaminants from the environment. Graphene, alone or in combination with other materials is one of the excellent adsorbents which earlier was applied as an adsorbent to remove organic material, arsenate, and heavy metal ions from water [24–26]. Moreover, graphene-based nanocomposite materials were recently used for treating water [27,28]. The good physical and chemical features of graphene, including its excellent SSA are important in terms of its application in adsorbing contaminants. The conventional approaches for preparing graphene provide an ultrafine powder. The SSA and good features of graphene depend on the nano-accumulation and lamellar stacking phenomena because of π–π and Van der Waals (VDW) interactions between graphene layers [29].

The magnetic properties of Fe_3O_4 provide its easy separation from aqueous media using a magnetic field, so it has attracted many attentions for applying as an adsorbent for removing contaminants from aqueous media [30]. A hybrid of Fe_3O_4 and Fe_2O_3 dispersed in biochar displays its ability to remove nitrate and fluoride from aqueous solution and magnetic separation [31]. Consequently, the current research is aimed to (a) study the efficiency and effectiveness of four nano-adsorbent (nano graphene, nano-Fe_3O_4, nano-clay, and ONCs) to nitrate adsorption and (b) examine the kinetics and isotherm of adsorbing nitrate from water using these four adsorbents.

2. Experimental

2.1. Materials

All chemicals used in this study were of analytical pure grade. Iron oxide nano-powder (Fe_3O_4), nano-clay montmorillonite (K10), graphene, stock solution of nitrate (1,000 mg L^{-1}) and hexadecyltrimethylammonium chloride (HDTMA-Cl) (formula: $C_{19}H_{42}CLN$, purity: 99% and molar weight = 320 g mol^{-1}) were prepared from Merck (Darmstadt, Germany), Sigma-Aldrich (Steinheim, Germany) or Fluka (Buchs, Switzerland).

2.2. Analysis and adsorption experiment

Nitrate solutions with different concentrations (30–200 mg L^{-1}) were prepared by diluting the stock solution. The tests were performed in 250 mL Erlenmeyer flasks in such a way that 100 mL of nitrate (30–200 mg L^{-1}) was poured into the flasks in each experiment. The primary pH of the solution was set to 7 and then, sufficient dosage of adsorbent (0.1 g) and nitrate solutions were poured into the Erlenmeyer flasks. All tests carried out at the temperature of 25°C. The solutions were stirred for 50 min at a stirring rate of 150 rpm. Then, the adsorbent was separated from the solutions by centrifuging at 5,000 rpm and then, the rest of the solution was filtered using a 0.45 μm cellulose filter. Amount of residual nitrate was determined using ultraviolet spectrophotometry technique (at 220 and 275 nm) [32] by a UV-VIS Double Beam Spectrophotometer (Shimadzu UV2800, Japan).

2.3. Preparation of modified nano-clay

Nano-clay was modified according to the method reported by Bandpei et al. [32]. In general, a solution of HDTMA-Cl surfactant (3 mMol L^{-1}) was poured into the 250 mL Erlenmeyer flasks. Next, 3 g of nano-clay was poured into all flasks. The samples were centrifuged after stirring 24 h using a shaker (20°C, 300 rpm and pH 7.0). Obtained materials were rinsed several times with pure water and then were put in an oven at 105°C to dry. Therefore, the modified nano-clay adsorbents were synthesized. Lastly, the synthesized adsorbents were stored in sealed polyethylene bottles. The schematic of the ONC synthesize is shown in Fig. 1.

In order to study kinetics, four nitrate solutions (100 mg L^{-1}) were prepared and four diverse adsorbents (0.1 g of each adsorbent) were added into the nitrate solution at the similar conditions of temperature and pH. The level of adsorbed nitrate was obtained by determining the concentration of the solution in intervals of 5 min using the beforementioned technique.

2.3.1. Characterization of synthesized ONC

The scanning electron microscopy (SEM) micrographs (Hitachi S-3000N, Japan) of the nano-clay and ONC samples are shown in Figs. 2a and b, respectively, which show an increase in porosity and the extensive surface of ONC

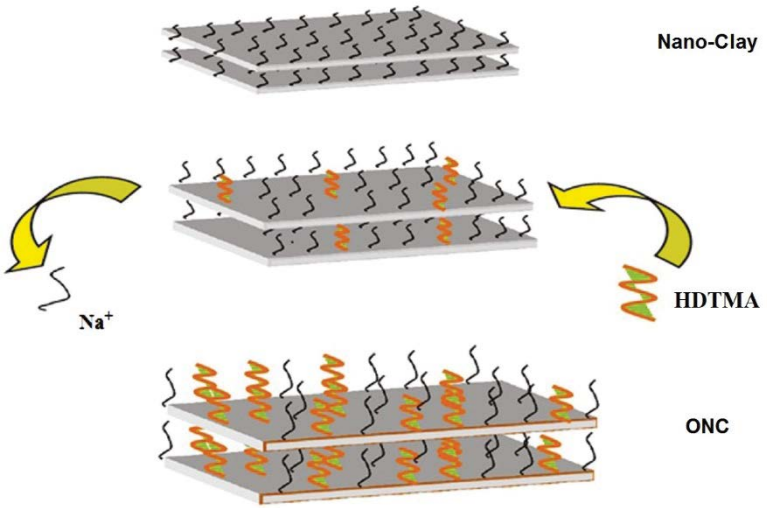

Fig. 1. Schematic of the ONC synthesize.

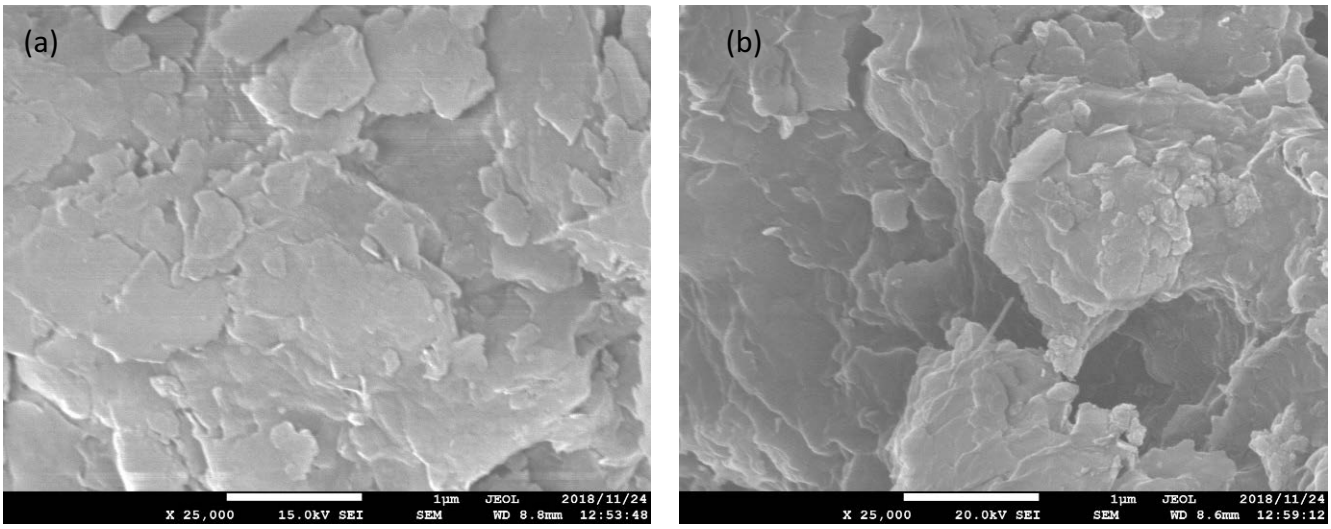

Fig. 2. SEM micrographs of (a) nano-clay and (b) ONC.

relative to nano-clay which can be attributed to the treatment of nano-clay with HDTMA-Cl surfactant. Also, the chemical compositions of the nano-clay and ONC were determined by the X-ray fluorescence (XRF) instrument (Shimadzu XRF-1800 with Rh radiation) and results are summarized in Table 1. Comparing the composition results of nano-clay and ONC, confirms the presence of carbon and chloride in the structure of modified nano-clay, which can be an evidence of successful synthesis of the ONC. The Brunauer–Emmett–Teller (BET) and Barrett–Joyner–Halenda (BJH) analysis were employed to measure the total area of the porous samples and calculate the distribution of pore size, respectively. The BET analysis results showed that the total SSA is equal to 4.46 $m^2\ g^{-1}$ and the total pore volume is 0.0068114 $cm^3\ g^{-1}$ for the nano-clay that is comparable with the total SSA (61.99 $m^2\ g^{-1}$) and the total pore volume (0.11 $cm^3\ g^{-1}$) for ONC. To determine the particle size of the sample, the BJH analysis was employed. The BJH analysis showed a mean pore diameter of 6.1 and 7.5 nm for the nano-clay and ONC, respectively (data are included in the supplementary).

The XRD charts of nano-clay and prepared ONC are shown in Fig. 3. The basal spacing of montmorillonite is identical with the value of 12.397 Å reported in the literature. The interaction between the surfactant and montmorillonite led to a shift of the d(001) diffraction peak of montmorillonite toward lower 2θ values, implying the expansion of the interlayer space due to the surfactant intercalation [33].

The TEM images before and after modification of nano-clay are shown in Fig. 4.

2.4. Isotherm and kinetic studies

Equilibrium adsorption isotherms can provide valuable result about the adsorption mechanism, features of the procedure and tendency of the adsorbent toward the target ion. Consequently, they can help to plan a more effective

adsorption system. In order to extract the investigated procedure isotherms, the adsorption outcomes were fitted into the adsorption isotherm models of Langmuir (Eq. (1)), Freundlich (Eq. (3)), Temkin (Eq. (4)), and Dubinin–Radushkevich (Eq. (5)).

$$\frac{1}{q_e}=\frac{1}{q_m}+\frac{1}{q_m K_L C_e} \tag{1}$$

Table 1
XRF analysis results for determination of composition the nano-clay and ONC

	%	
Constituent	Nano-clay	ONC
C	0	37.23
O	37.75	35.84
Fe	7.16	7.07
Na	1.91	0.93
Mg	1.4	0.8
Al	14.75	5.81
Si	34.28	11.03
K	1.41	0
Ca	1.34	0
Cl^-	0	1.19
Co	0	0.1

$$R_L=\frac{1}{\left[1+bC_0\right]} \tag{2}$$

$$\log q_e=\log K_f+\frac{1}{n}\log C_e \tag{3}$$

$$q_e=\frac{RT}{b_T}\ln K_T+\left(\frac{RT}{b_T}\right)\ln C_e \tag{4}$$

$$\ln q_e=\ln q_s-\left(K_{\mathrm{ad}}\varepsilon^2\right) \tag{5}$$

$$\varepsilon=RT\ln\left(1+\frac{1}{C_e}\right) \tag{6}$$

In Eqs. (1)–(5), q_e (mg g^{-1}) represents the amount of the nitrate ions adsorbed at equilibrium, C_e (mg L^{-1}) is the equilibrium concentration of nitrate in the solution, q_m (mg g^{-1}) is the highest capacity of the adsorbent for ions monolayer adsorption, b (L mg^{-1}) is the Langmuir constant relating with binding energy, and C_0 (mg L^{-1}) refers to the primary amount of nitrate [34]. The amounts of C_0 and b can be applied for calculating the R_L parameter according to Eq. (2). R_L unravels whether an adsorption procedure is irreversible ($R_L = 0$), linear ($R_L = 1$), unfavorable ($R_L > 1$), or favorable ($0 < R_L < 1$). In the Freundlich model (Eq. (3)), $1/n$ refers to the intensity of the adsorption and K_f (mg g^{-1}) represents adsorption capacity for the adsorbent [34]. The $1/n$ values smaller than 1 are related

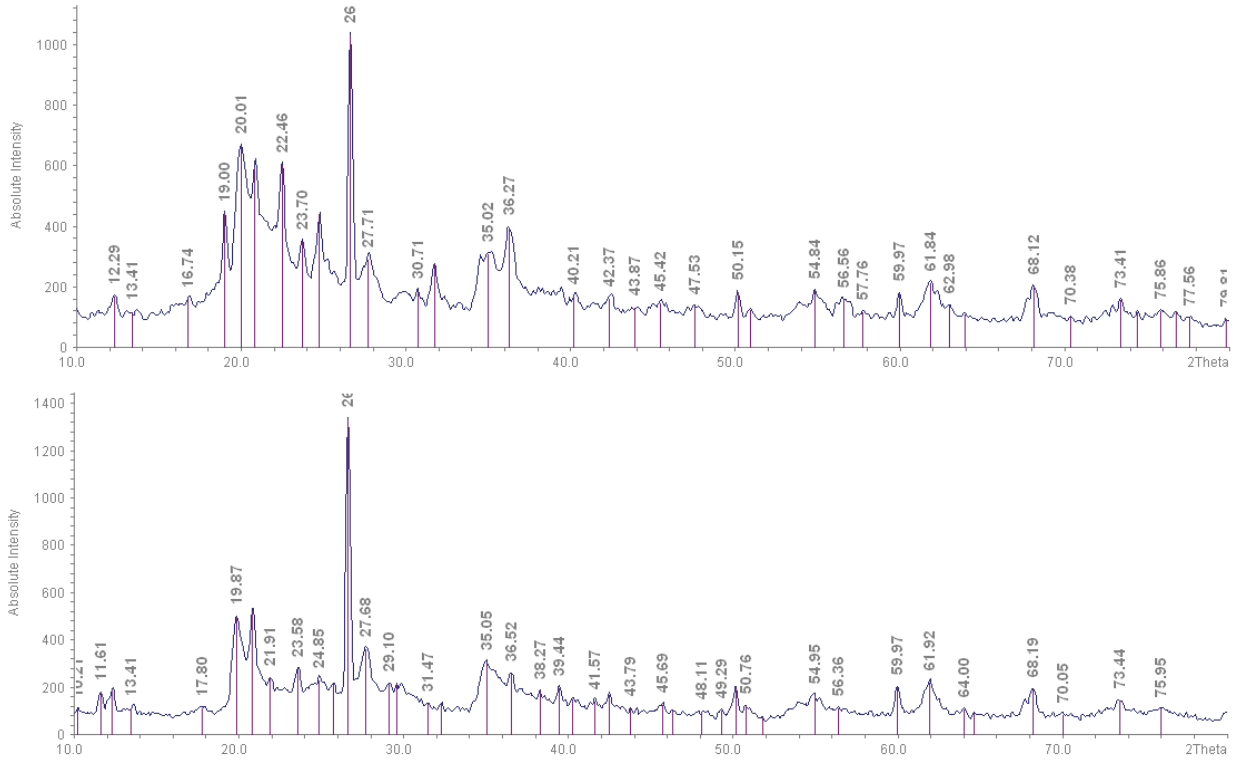

Fig. 3. XRD analysis of nano-clay (top) and modified nano-clay (down).

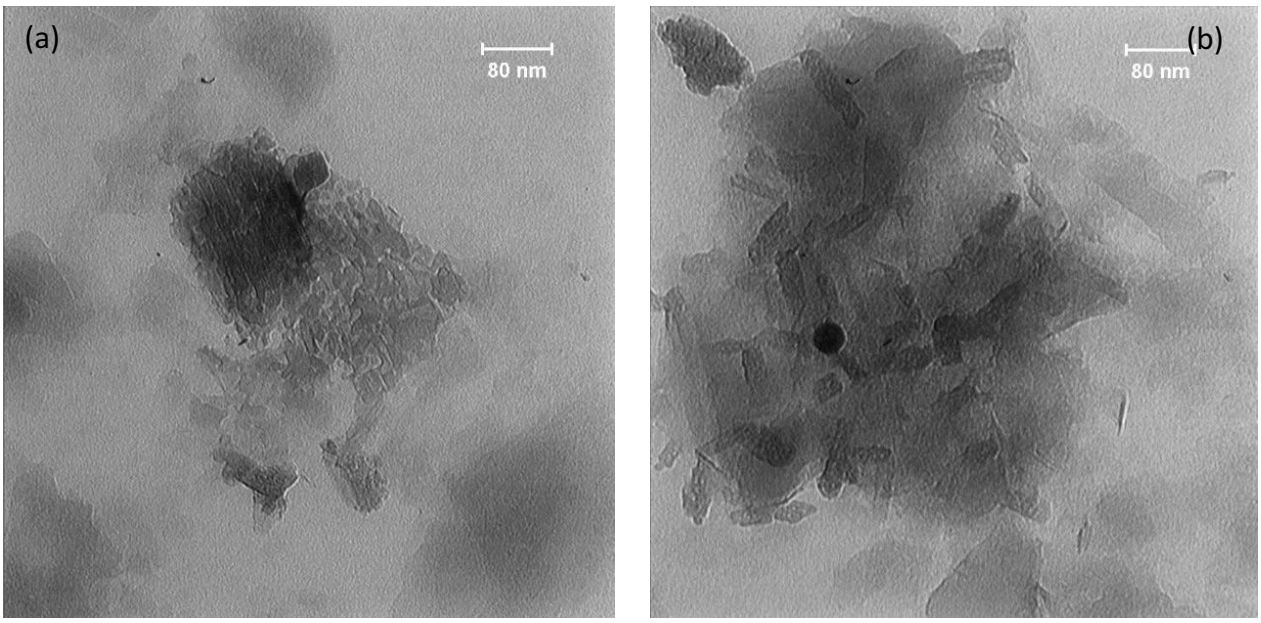

Fig. 4. TEM image of (a) nano-clay and (b) ONC.

to standard adsorption and 1/*n* values is between 1 and 10 signify a favorable adsorption procedure [35]. In Eq. (4), the Temkin model takes into account the influences of several indirect adsorbent–adsorbate interactions on the adsorption isotherms and suggests a linear decrease in the adsorption heat of the adsorption layer for all adsorbates with covering. In this equation, K_T (L g^{-1}) is the Temkin parameter that defines the highest binding energy at equilibrium and b_T (J mol^{-1}) refers to a constant factor for adsorption heat [36]. Meantime, a large b_T value shows rapid adsorption of the adsorbate at the first step of the procedure, a small value of K_T shows weak bonding of the adsorbate into the adsorbent.

In Eq. (5), the Dubinin–Radushkevich model is used to describe the mechanism of adsorption with a Gaussian energy distribution onto a heterogeneous surface, where q_s refers to the theoretical isotherm saturation capacity (mg g^{-1}) and K_{ad} represents the Dubinin–Radushkevich isotherm constant (mg^2 kJ^{-2}), R represents the universal gas constant (8.314 J K^{-1} mol^{-1}) and T refers to the temperature (K).

In order to study the kinetics of the adsorption procedure, the linear form equation of pseudo-first-order (Eq. (7)), pseudo-second-order (Eq. (8)) and intra-particle diffusion (Eq. (9)) models were studied:

$$\log q_e - q_t = \log q_e - \frac{k_1}{2.303} t \tag{7}$$

$$\frac{t}{q_t} = \frac{1}{k_2 \times q_e^2} + \frac{1}{q_e} \times t \tag{8}$$

$$q_t = K_d t^{1/2} + I \tag{9}$$

where q_e (mg g^{-1}) and q_t (mg g^{-1}) represent the concentration of nitrate adsorbed on the adsorbent at equilibrium and time t (min), respectively, k_1 (min^{-1}) is the pseudo-first-order rate constant and k_2 (g mg^{-1} min^{-1}) refers to the pseudo-second-order rate constant of adsorption [37]. Lastly, K_d is the rate constant corresponding to intra-particle diffusion (mg g^{-1} min$^{-1/2}$) and I, refers to a constant, which defines the boundary layer thickness.

3. Results and discussion

3.1. Adsorption isotherms

As above-mentioned, the experimental data were fitted into four isotherm models. Table 2, which represents the achieved isotherm parameters, shows an increase in the highest capacity of the adsorbent particles (q_m) from 44.64 to 243.90 mg g^{-1} with altering the type of adsorbent from graphene to modified nano-clay. The notable increase in the adsorption capacity after modification of nano-clay with HDTMA may be attributed to the electrostatic interactions between the nitrate ion (negatively charged) and the modified nano-clay with the surfactant cations [38]. Also the increase in interlayer spacing because of intercalation of surfactant and increase in SSA increases the adsorption capacity of ONC [39]. Furthermore, Fig. 5 shows the level of nitrate adsorbed by diverse adsorbents at diverse initial nitrate amounts. Fig. 6 shows adsorption isotherms for (a) Langmuir, (b) Freundlich, (c) Temkin, and (d) Dubinin–Radushkevich for different adsorbents. As K_f is the potential of nitrate adsorption on the adsorbent, the increase of this factor by altering the adsorbent suggests the involvement of the heterogeneous sites of the adsorbent particles in the adsorption process. To assure the involvement of heterogeneous adsorption sites in the procedure, the Temkin isotherm was used. According to this isotherm, large values of the equilibrium binding constant (K_T) signify strong adsorbate–adsorbent bonding, but large value of adsorption heat (b_T)

Table 2
Isotherm parameters corresponding to nitrate adsorption onto different adsorbents

Isotherm model	Parameter	Standard deviation of each parameter for different adsorbents (STDEV)							
		Graphene	STDEV	Fe_3O_4	STDEV	Clay	STDEV	ONC	STDEV
Langmuir	q_m (mg g^{-1})	44.64	1.89	81.30	2.02	112.35	4.88	243.90	7.53
	K_L (L mg^{-1})	0.019	0.00	0.011	0.00	0.011	0.00	0.016	0.00
	R_L	0.634	0.021	0.745	0.024	0.745	0.024	0.671	0.023
	R^2	0.964	0.029	0.965	0.033	0.9794	0.032	0.9852	0.035
Freundlich	K_f (mg g^{-1})	0.0630	0.0044	0.1593	0.0085	0.1952	0.0094	0.1082	0.0037
	n	0.43339	0.0017	0.5636	0.0202	0.6649	0.0246	0.8036	0.0265
	R^2	0.8660	0.0346	0.8793	0.0360	0.9048	0.0325	0.9258	0.0342
Temkin	K_T (L g^{-1})	0.3378	0.0145	0.1916	0.0072	0.1543	0.0063	0.2263	0.0075
	b_T (J mol^{-1})	6.806	0.2178	12.264	0.5519	21.302	0.9586	51.757	2.2773
	R^2	0.9344	0.0364	0.9513	0.0390	0.9501	0.0371	0.9835	0.0384
Dubinin–Radushkevich	q_s (mg g^{-1})	24.955	1.1230	36.689	1.1741	53.608	2.1979	105.204	2.9457
	R^2	0.9760	0.038	0.9587	0.0431	0.9004	0.041	0.8779	0.0316
	K_{ad} (mg^2 J^{-2})	0.00005	0.0000	0.00006	0.00000	0.00005	0.00000	0.00001	0.00000

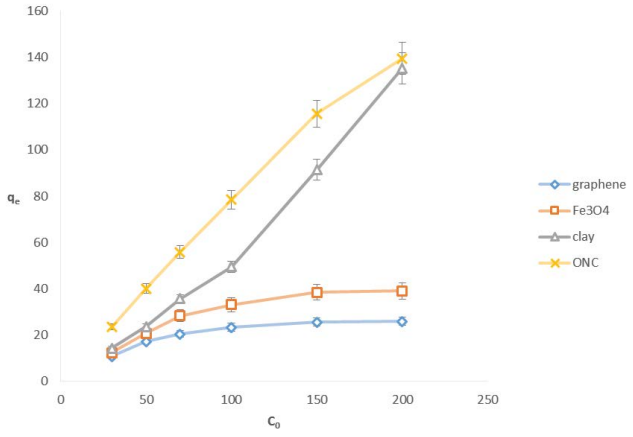

Fig. 5. Comparison of the amount of nitrate adsorbed by diverse adsorbents at different initial nitrate concentrations.

shows fast adsorption at the initial step of the procedure. The minimum K_T is related to nano-clay (the weakest adsorbate–adsorbent bonding that causes its easier recovery following adsorption comparing with other adsorbents) and the maximum b_T values of modified nano-clay (which shows faster adsorption procedure than other adsorbents). Consequently, performing the adsorption procedure by nano-clay can cause the weakest ion–adsorbate bonding and most of the nitrate is adsorbed at the first step by using modified nano-clay. The results of comparison of the correlation coefficients of adsorption isotherms indicated that graphene matches better with the Dubinin–Radushkevich model, however, three other adsorption procedures fit with the Langmuir model.

3.2. Kinetic study

As investigating the kinetics of water treatment procedures offers some insight about the associated mechanism, the adsorption system kinetics is studied through fitting the obtained time profiles into the pseudo-first-order (PFO), pseudo-second-order (PSO), and intra-particle diffusion (IPD) kinetics models. By using the PSO model, it was supposed that the nitrate ions adsorb onto two non-similar sites and the rate determination step (RDS) contribute in sharing or exchanging electron between the adsorbent particles and the ions. Table 3 shows the kinetic parameters for these three models. Fig. 7 displays the diagrams of three kinetics models used for adsorbing nitrate using diverse adsorbents. Adsorbing nitrate on graphene fits completely with the pseudo-second-order model and IPD model with two straight lines demonstrating two steps impact on the sorption procedure. It is supposed that the external resistance to mass transfer of surrounding the particles is considerable only in the initial steps of adsorption: this is showed by the first sharper portion of the graph. The second linear portion is the gradual adsorption step with controlling diffusion of intra-particle [40]. Nano-Fe_3O_4 adsorption procedure follows both first-order and second-order models. The IPD model fits completely with the adsorption using nano-clay with a straight line, representing that the sorption procedure is affected by the diffusion of intra-particle. Both pseudo-second-order model and IPD model can be applied for describing the sorption kinetics when ONC is adsorbent. Two straight lines observed in the IPD model shows that two steps involve in the adsorption procedure. The kinetics data of the IPD model were evaluated to unravel the diffusion roles, chemical reaction, and mass transfer events in adsorbing nitrate by the adsorbents and determining the RDS. Based on this model, if the diagram of q vs. $t^{0.5}$ is linear, then the examined procedure depends on IPD, and IPD is the only RDS when the resultant line intersects the origin of the plot. Furthermore, if there are multiple linear plots associated with different steps, then more than one IPD step impacts on the adsorption procedure. The charts of graphene and ONC (Fig. 7c) are multi-linear, so the adsorption procedure includes two IPD steps. The first step of the procedure is an external or instantaneous adsorption reaction that reveals as the steeper

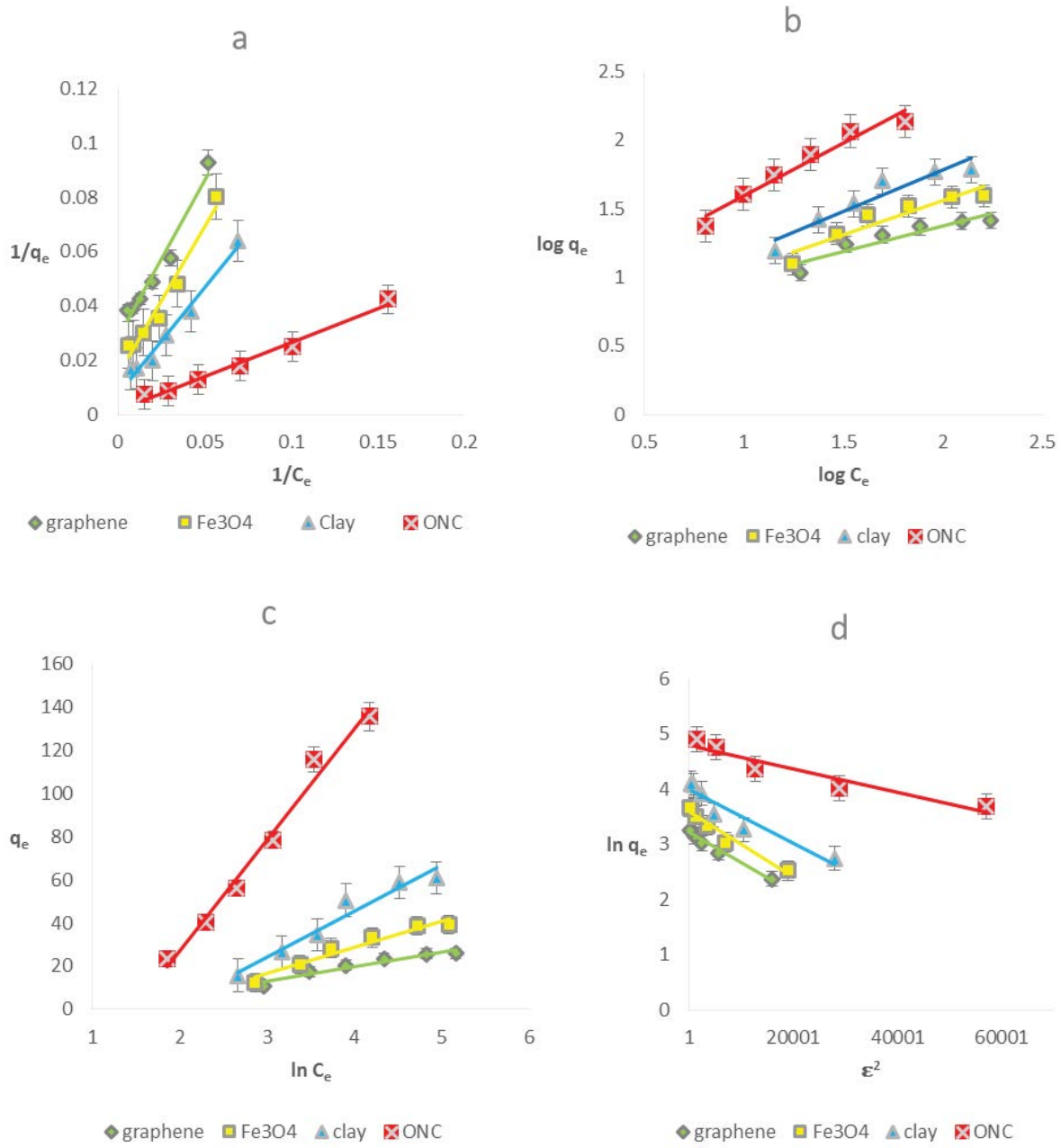

Fig. 6. Adsorption isotherms: (a) Langmuir, (b) Freundlich, (c) Temkin, and (d) Dubinin–Radushkevich for different adsorbents.

portions of the plots (Fig. 7c graphene 1 and ONC 1), however the second step is associated with diffusion of the ions toward the pores as the RDS is observed as the linear parts of the plots (Fig. 7c graphene 2 and ONC2). The plots plateaus, where IPD begins to slow down because of the reduction of available nitrate, can be taken into account as the last step, that is, equilibrium. Consequently, external surface adsorption influenced on the adsorption of the nitrate ions onto the suggested adsorbent and IPD is the RSD. Moreover, the positive sign of I and the lower value of K_d for the IPD stage vs. external surface adsorption stage illustrates that the diffusion stage involves a quicker ion transfer and the boundary layer impacts the adsorption rate.

4. Conclusions

Application of four diverse adsorbents (graphene, nano-Fe_3O_4, nano-clay, and ONC) was studied in terms of their ability to adsorb nitrate from water. Graphene fits well with the Dubinin–Radushkevich model; however three other adsorption procedures match with the Langmuir model. Furthermore, the highest adsorption capacity (q_m) is 44.64, 81.30, 112.35, and 243.90 mg g^{-1} for graphene, nano-Fe_3O_4, nano-clay, and ONC, respectively. Comparing the Temkin isotherms for diverse adsorbents, the equilibrium binding constant (K_T) values determined 0.3378, 0.1916, 0.1543, and 0.2263 L g^{-1} for graphene, nano-Fe_3O_4, nano-clay, and ONC,

Table 3
Kinetic parameters for the adsorption procedure at different adsorbents (initial amount of nitrate, C_0 = 100 mg L^{-1})

Adsorbents	Pseudo-first-order			Pseudo-second-order			Intra-particle diffusion					
							First line (surface diffusion)			Second line (intra-particle diffusion)		
	q_e (mg g^{-1})	k_1 (min^{-1}) × 10^{-3}	R^2	q_e (mg g^{-1})	k_2 (g mg^{-1} min^{-1}) × 10^{-3}	R^2	K_d (mg g^{-1} $min^{-1/2}$)	I (mg g^{-1})	R^2	K_d (mg g^{-1} $min^{-1/2}$)	I (mg g^{-1})	R^2
Graphene	24.96	7.80	0.98	33.45	2.05	0.99	4.66	1.46	0.99	1.29	15.53	0.78
Nano-Fe_3O_4	27.68	51.36	0.99	40.16	2.15	0.99	4.74	3.25	0.98	–	–	–
Nano-clay	48.27	73.24	0.94	61.72	1.54	0.97	6.83	8.58	0.98	–	–	–
ONC	108.89	115.15	0.95	107.53	0.75	0.99	18.08	10.02	0.99	7.73	33.28	0.99

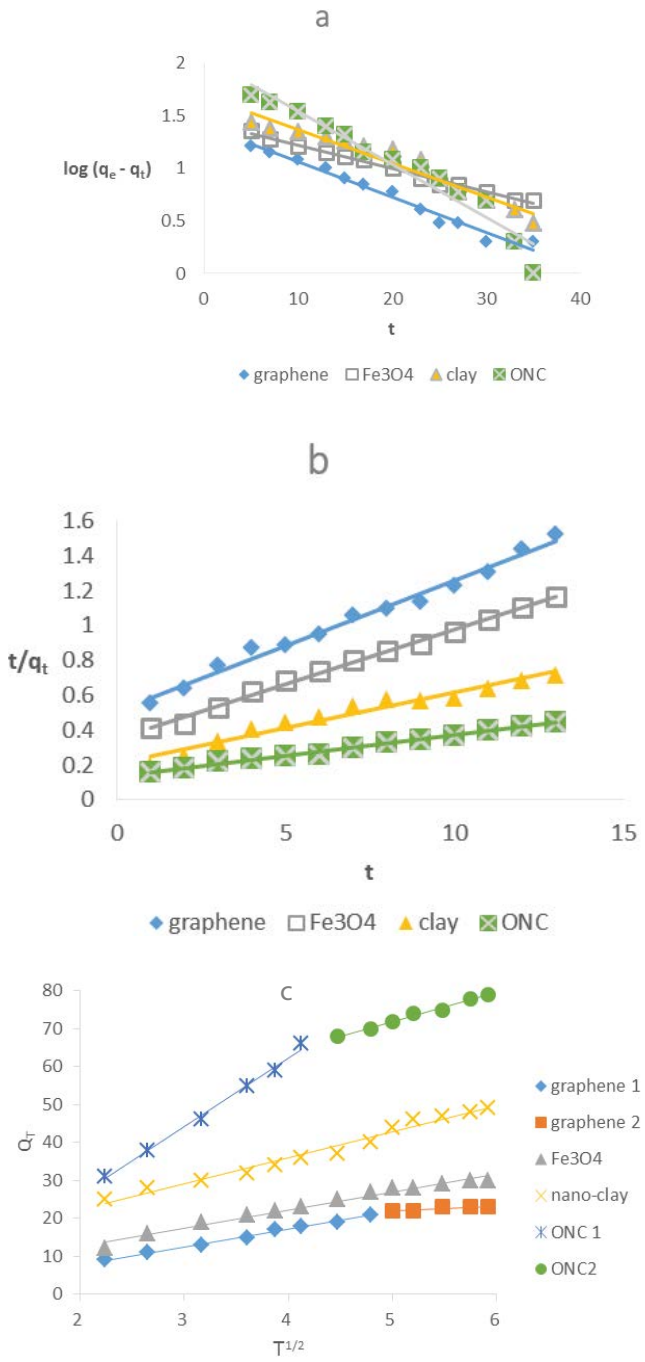

Fig. 7. Kinetics corresponding to nitrate adsorption by diverse adsorbent based on (a) pseudo-first-order, (b) pseudo-second-order, and (c) intra-particle diffusion kinetic models.

respectively, that shows the strength of nitrate binding to adsorbent differs as: graphene > ONC > nano-Fe_3O_4 > nano-clay. It is valuable for understanding the probability of separating adsorbed ions from adsorbent and adsorbent recovery in designing a novel adsorbent.

PFO, PSO, and IPD kinetic models were used to study kinetics. Adsorption of nitrate on graphene fits well with the PSO model and also with the IPD model. Nano-Fe_3O_4 adsorption procedure conforms to both PFO and PSO models.

The IPD model is in a good agreement with the adsorption using nano-clay and ONC follows both PSO and IPD model for describing the sorption kinetics. Correspondingly, respecting the PFO model, the unimolecular rate constant (k_1) enhances from graphene to ONC, which proves the experimental results.

In conclusion, the sequence corresponding to q_m was obtained as the subsequent by altering the adsorbents: graphene < nano-Fe_3O_4 < nano-clay < ONC. Also based on the PFO model and comparison of kinetics constant (k_1), the order of adsorption speed was graphene < nano-Fe_3O_4 < nano-clay < ONC. Before modification of nano clay with HDTMA, plates in nano-clay are near each other. After adding HDTMA, plates are separated and more room is available for nitrate ions to diffuse more easily between sheets and to be adsorbed. SEM and TEM images also show an increase in the porosity of ONC which caused an increase in adsorption. The intercalation or grafting of organic molecules may eventually increase the interspace layer spacing of clay and hence possessed with higher SSA and the affinity toward several pollutants present in aqueous solution [41]. Consequently, the ONC may be used as a good adsorbent for nitrate removal from aqueous solution.

List of symbols and abbreviations

Symbols

ONC	—	Organically modified nano-clay
q_m	—	Highest adsorbent capacity
PFO	—	Pseudo-first-order
PSO	—	Pseudo-second-order
IPD	—	Intra-particle diffusion
WHO	—	World Health Organization
SSA	—	Specific surface area
VDW	—	Van der Waals
HDTMA-Cl	—	Hexadecyltrimethylammonium chloride
SEM	—	Scanning electron microscopy
XRF	—	X-ray fluorescence
BET	—	Brunauer–Emmett–Teller
BJH	—	Barrett–Joyner–Halenda
q_e	—	Amount of the nitrate ions adsorbed at equilibrium
C_e	—	Equilibrium concentration of Nitrate in the solution
C_0	—	Primary concentration of Nitrate
R_L	—	Reversibility parameter
$1/n$	—	Intensity of the adsorption
K_f	—	Adsorption capacity
K_T	—	Temkin parameter
b_T	—	Constant factor for adsorption heat
q_s	—	Theoretical isotherm saturation capacity
T	—	Temperature, K
q_t	—	Concentration of nitrate adsorbed on the adsorbent at time t, min
k_1	—	Pseudo-first-order rate constant
k_2	—	Pseudo-second-order rate constant of adsorption
K_d	—	Rate constant corresponding to intra-particle diffusion
I	—	Constant related to boundary layer thickness

References

[1] P. Weiss, E.C. Waldroup, J. Williams, M. Sweeney, J. Ren, Eutrophication and causation: an investigation of potassium nitrate and algae growth, J. Introductory Biol. Invest., 5 (2016) 3.

[2] S.F. Johnson, Methemoglobinemia: Infants at Risk, Current Problems in Pediatric and Adolescent Health Care, Elsevier, 49 (2019) 57–67.

[3] C. Tociu, E. Marcu, I.E. Ciobotaru, C. Maria, Risk assessment of population exposure to nitrates/nitrites in groundwater: a case study approach, Environ. Res. Prot., 13 (2016) 39–45.

[4] J.D. Brender, P.J. Weyer, Agricultural compounds in water and birth defects, Curr. Environ. Health Rep., 3 (2016) 144–152.

[5] J.-Y. Jeong, H.-K. Kim, J.-H. Kim, J.-Y. Park, Electrochemical removal of nitrate using ZVI packed bed bipolar electrolytic cell, Chemosphere, 89 (2012) 172–178.

[6] M.L. Bosko, M. Rodrigues, J.Z. Ferreira, E.E. Miró, A.M. Bernardes, Nitrate reduction of brines from water desalination plants by membrane electrolysis, J. Membr. Sci., 451 (2014) 276–284.

[7] J. Bohdziewicz, M. Bodzek, E. Wąsik, The application of reverse osmosis and nanofiltration to the removal of nitrates from groundwater, Desalination, 121 (1999) 139–147.

[8] A. Keränen, T. Leiviskä, B.-Y. Gao, O. Hormi, J. Tanskanen, Preparation of novel anion exchangers from pine sawdust and bark, spruce bark, birch bark and peat for the removal of nitrate, Chem. Eng. Sci., 98 (2013) 59–68.

[9] B. Ovez, S. Ozgen, M. Yuksel, Biological denitrification in drinking water using *Glycyrrhiza glabra* and *Arunda donax* as the carbon source, Process Biochem., 41 (2006) 1539–1544.

[10] X. Wang, J. Wang, Removal of nitrate from groundwater by heterotrophic denitrification using the solid carbon source, Sci. China, Ser. B Chem., 52 (2009) 236–240.

[11] C.A. Bode-Aluko, O. Pereao, G. Ndayambaje, L. Petrik, Adsorption of toxic metals on modified polyacrylonitrile nanofibres: a review, Water Air Soil Pollut., 228 (2017) 35.

[12] S. Mintova, N.H. Olson, V. Valtchev, T. Bein, Mechanism of zeolite A nanocrystal growth from colloids at room temperature, Science, 283 (1999) 958–960.

[13] S.C. Larsen, Nanocrystalline zeolites and zeolite structures: synthesis, characterization, and applications, J. Phys. Chem. C, 111 (2007) 18464–18474.

[14] D. Afzali, A. Mostafavi, M. Mirzaei, Preconcentration of gold ions from water samples by modified organo-nanoclay sorbent prior to flame atomic absorption spectrometry determination, J. Hazard. Mater., 181 (2010) 957–961.

[15] S. Awate, K. Suzuki, Enhanced adsorption capacity and photocatalytic oxidative activity of dyes in aqueous medium by hydrothermally treated titania pillared clay, Adsorption, 7 (2001) 319–326.

[16] H. Wang, B.A. Holmberg, Y. Yan, Homogeneous polymer–zeolite nanocomposite membranes by incorporating dispersible template-removed zeolite nanocrystals, J. Mater. Chem., 12 (2002) 3640–3643.

[17] S. Mallakpour, M. Dinari, Preparation and characterization of new organoclays using natural amino acids and Cloisite Na^+, Appl. Clay Sci., 51 (2011) 353–359.

[18] S. Mallakpour, M. Dinari, Biomodification of cloisite Na^+ with L-methionine amino acid and preparation of poly (vinyl alcohol)/organoclay nanocomposite films, J. Appl. Polym. Sci., 124 (2012) 4322–4330.

[19] S. Mallakpour, M. Dinari, Novel nanocomposites based on reactive organoclay of l-tyrosine and amine end-capped poly (amide–imide): synthesis and characterization, Appl. Clay Sci., 75 (2013) 67–73.

[20] I. Calabrese, G. Cavallaro, G. Lazzara, M. Merli, L. Sciascia, M.L.T. Liveri, Preparation and characterization of bio-organoclays using nonionic surfactant, Adsorption, 22 (2016) 105–116.

[21] A. Khenifi, Z. Bouberka, F. Sekrane, M. Kameche, Z. Derriche, Adsorption study of an industrial dye by an organic clay, Adsorption, 13 (2007) 149–158.

[22] S. Dal Bosco, R. Jimenez, C. Vignado, J. Fontana, B. Geraldo, F. Figueiredo, D. Mandelli, W. Carvalho, Removal of Mn (II)

and Cd (II) from wastewaters by natural and modified clays, Adsorption, 12 (2006) 133–146.
[23] K.G. Bhattacharyya, S.S. Gupta, Adsorption of Fe (III) from water by natural and acid activated clays: studies on equilibrium isotherm, kinetics and thermodynamics of interactions, Adsorption, 12 (2006) 185–204.
[24] Q. Fang, X. Zhou, W. Deng, Y. Liu, Z. Zheng, Z. Liu, Nitrogen-doped graphene nanoscroll foam with high diffusion rate and binding affinity for removal of organic pollutants, Small, 13 (2017) 1603779.
[25] S. Lath, D. Navarro, D. Tran, A. Kumar, D. Losic, M.J. McLaughlin, Mixed-mode remediation of cadmium and arsenate ions using graphene-based materials, CLEAN Soil Air Water, 46 (2018) 1800073.
[26] G. Yu, Y. Lu, J. Guo, M. Patel, A. Bafana, X. Wang, B. Qiu, C. Jeffryes, S. Wei, Z. Guo, E.K. Wujcik, Carbon nanotubes, graphene, and their derivatives for heavy metal removal, Adv. Compos. Hybrid Mater., 1 (2018) 56–78.
[27] P.S. Kumar, P. Yaashikaa, S. Ramalingam, Efficient Removal of Nitrate and Phosphate using Graphene Nanocomposites, A New Generation Material Graphene: Applications in Water Technology, Springer, Cham, 2019, pp. 287–307
[28] Y. Cao, X. Li, Adsorption of graphene for the removal of inorganic pollutants in water purification: a review, Adsorption, 20 (2014) 713–727.
[29] L. Wu, Z. Qin, L. Zhang, T. Meng, F. Yu, J. Ma, CNT-enhanced amino-functionalized graphene aerogel adsorbent for highly efficient removal of formaldehyde, New J. Chem., 41 (2017) 2527–2533.
[30] M. Dinari, R. Tabatabaeian, Ultra-fast and highly efficient removal of cadmium ions by magnetic layered double hydroxide/guargum bionanocomposites, Carbohydr. Polym., 192 (2018) 317–326.
[31] N.B. Dewage, A.S. Liyanage, C.U. Pittman Jr., D. Mohan, T. Mlsna, Fast nitrate and fluoride adsorption and magnetic separation from water on α-Fe_2O_3 and Fe_3O_4 dispersed on Douglas fir biochar, Bioresour. Technol., 263 (2018) 258–265.
[32] A.M. Bandpei, S.M. Mohseni, A. Sheikhmohammadi, M. Sardar, M. Sarkhosh, M. Almasian, M. Avazpour, Z. Mosallanejad, Z. Atafar, S. Nazari, Optimization of arsenite removal by adsorption onto organically modified montmorillonite clay: experimental & theoretical approaches, Korean J. Chem. Eng., 34 (2017) 376–383.
[33] L. Zhou, H. Chen, X. Jiang, F. Lu, Y. Zhou, W. Yin, X. Ji, Modification of montmorillonite surfaces using a novel class of cationic gemini surfactants, J. Colloid Interface Sci., 332 (2009) 16–21.
[34] R. Ahmad, A. Mirza, Synthesis of Guar gum/bentonite a novel bionanocomposite: isotherms, kinetics and thermodynamic studies for the removal of Pb (II) and crystal violet dye, J. Mol. Liq., 249 (2018) 805–814.
[35] M. Massoudinejad, M. Ghaderpoori, A. Shahsavani, A. Jafari, B. Kamarehie, A. Ghaderpoury, M.M. Amini, Ethylenediamine-functionalized cubic ZIF-8 for arsenic adsorption from aqueous solution: modeling, isotherms, kinetics and thermodynamics, J. Mol. Liq., 255 (2018) 263–268.
[36] M. Massoudinejad, M. Ghaderpoori, A. Shahsavani, M.M. Amini, Adsorption of fluoride over a metal organic framework Uio-66 functionalized with amine groups and optimization with response surface methodology, J. Mol. Liq., 221 (2016) 279–286.
[37] E. Ahmadi, S. Yousefzadeh, M. Ansari, H.R. Ghaffari, A. Azari, M. Miri, A. Mesdaghinia, R. Nabizadeh, B. Kakavandi, P. Ahmadi, Performance, kinetic, and biodegradation pathway evaluation of anaerobic fixed film fixed bed reactor in removing phthalic acid esters from wastewater, Sci. Rep., 7 (2017) 41020.
[38] Y. Xi, M. Mallavarapu, R. Naidu, Preparation, characterization of surfactants modified clay minerals and nitrate adsorption, Appl. Clay Sci., 48 (2010) 92–96.
[39] M. Ge, X. Wang, M. Du, G. Liang, G. Hu, S.M. Jahangir Alam, Adsorption analyses of phenol from aqueous solutions using magadiite modified with organo-functional groups: kinetic and equilibrium studies, Materials, 12 (2019) 96.
[40] V. Fierro, V. Torné-Fernández, D. Montané, A. Celzard, Adsorption of phenol onto activated carbons having different textural and surface properties, Microporous Mesoporous Mater., 111 (2008) 276–284.
[41] S.M. Lee, D. Tiwari, Organo and inorgano-organo-modified clays in the remediation of aqueous solutions: an overview, Appl. Clay Sci., 59 (2012) 84–102.

Supplementary information

Table S1
BET analysis parameters before modification

Starting point	8	
End point	15	
Slope (Linear)	0.7033	
Intercept (Linear)	0.2726	
Correlation coefficient	0.9917	
V_m	1.0247	(cm^3 (STP) g^{-1})
$a_{s,BET}$	4.46	(m^2 g^{-1})
C	3.5804	
Total pore volume (p/p_0 = 0.990)	0.0068114	(cm^3 g^{-1})
Mean pore diameter	6.1089	(nm)

Table S2
BET analysis parameters after modification

Starting point	5	
End point	6	
Slope (Linear)	0.069923	
Intercept (Linear)	0.0002842	
Correlation coefficient	1	
V_m	14.244	(cm^3 (STP) g^{-1})
$a_{s,BET}$	61.995	(m^2 g^{-1})
C	247.03	
Total pore volume (p/p_0 = 0.990)	0.1163	(cm^3 g^{-1})
Mean pore diameter	7.5032	(nm)

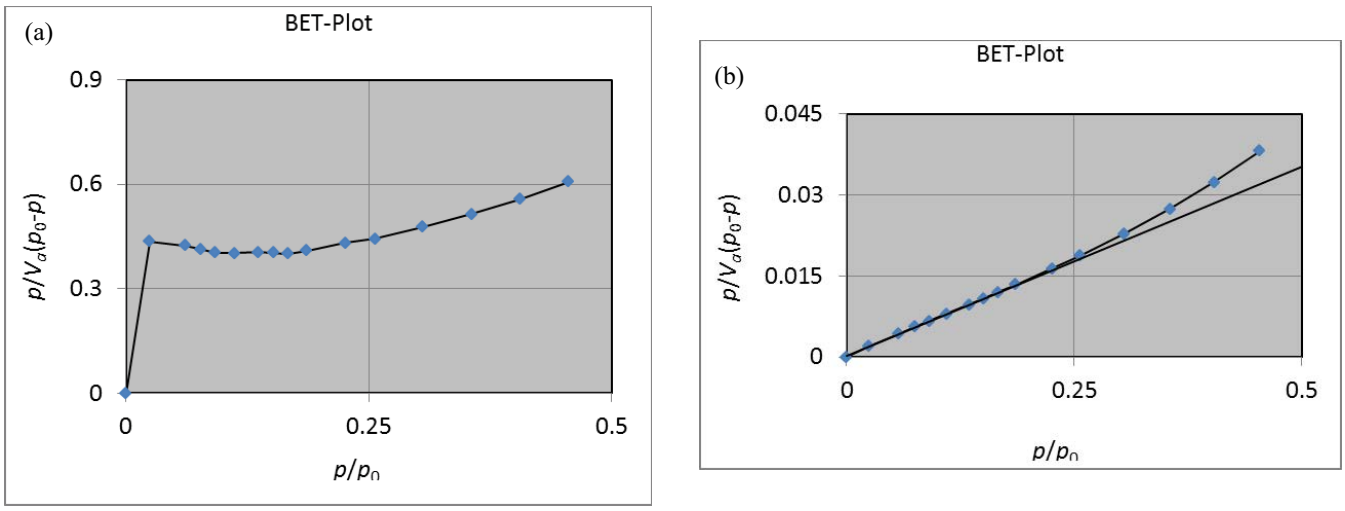

Fig. S1. BET analysis on nano-clay (a) before and (b) after modification.

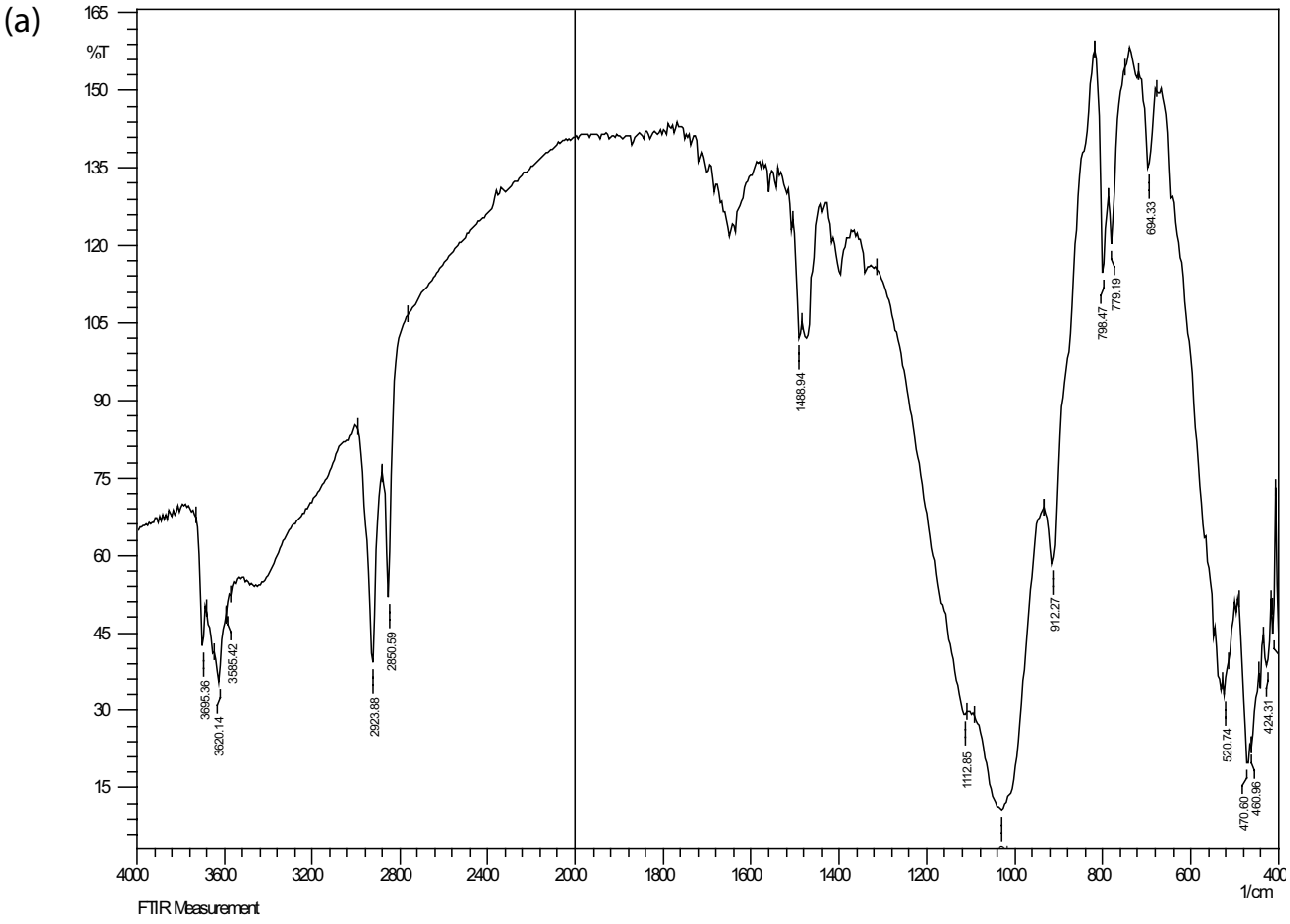

Fig. S2. *Continued*.

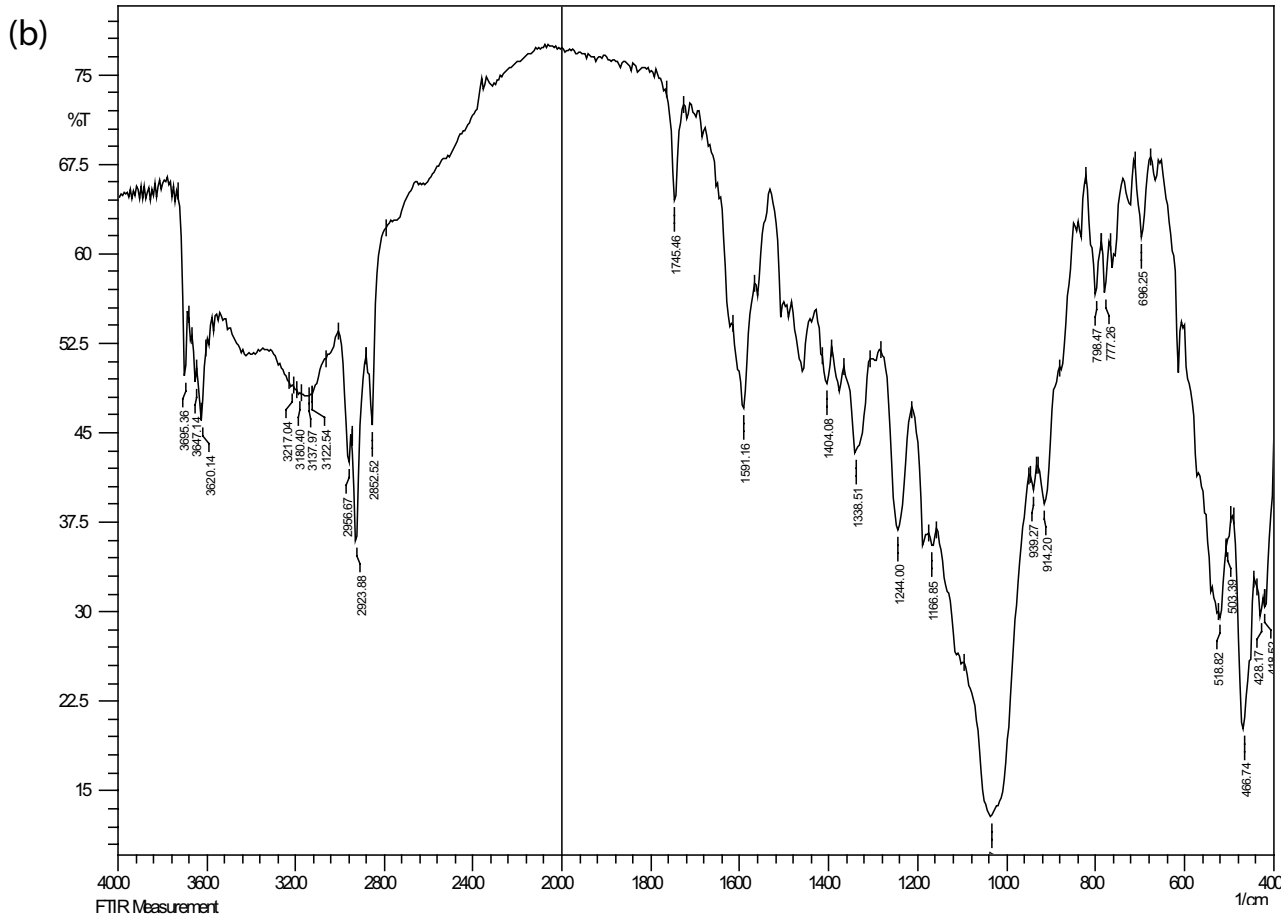

Fig. S2. FTIR analysis of (a) nano-clay and (b) ONC.

Some characterization of other adsorbents: (a) Graphene, and (b) Fe_3O_4.

(a) Graphene:
Research grade graphene nano-platelets powder
Purity: 99.5% – Graphene
Thickness: 2–18 nm, Less than 32 layers
pH: 7–7.7 (30°C)
Volume resistivity: 4×10^{-4} ohm cm
Diameter: 4–12 um
SSA: 500–1,200 $m^2\ g^{-1}$

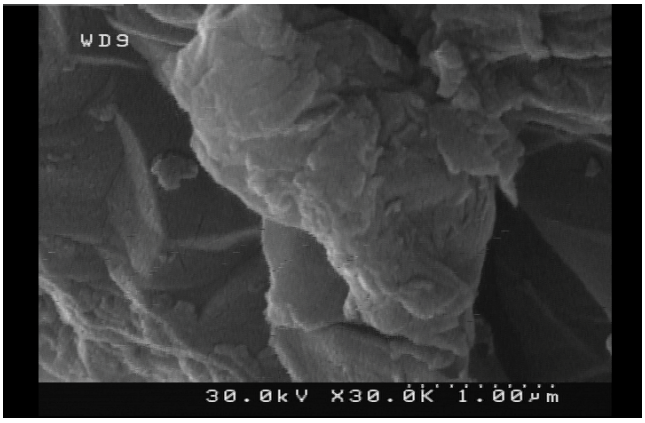

Fig. S3. SEM analysis of graphene.

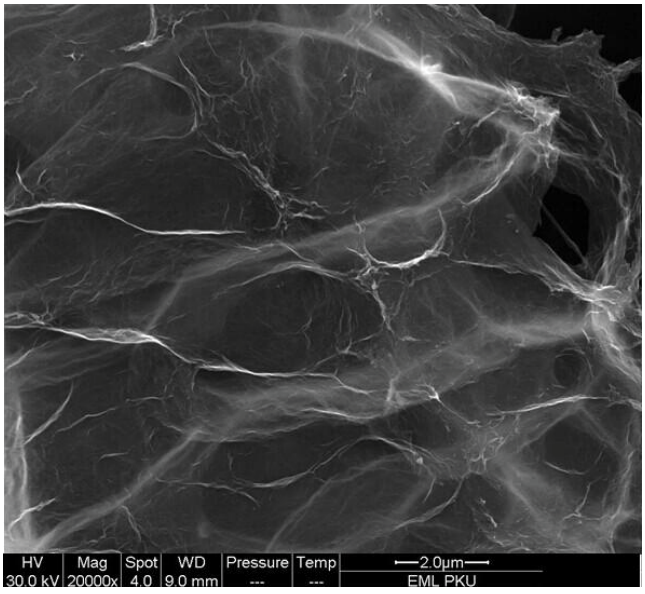

Fig. S4. TEM analysis of graphene.

(b) Nano-Fe_3O_4

Nanopowder (Fe_3O_4) purity: 98%
APS: 20–30 nm
SSA: 40–60 $m^2\ g^{-1}$
Color: dark brown
Morphology: spherical
Bulk density: 0.84 g cm^{-3}
True density: 4.8–5.1 g cm^{-3}

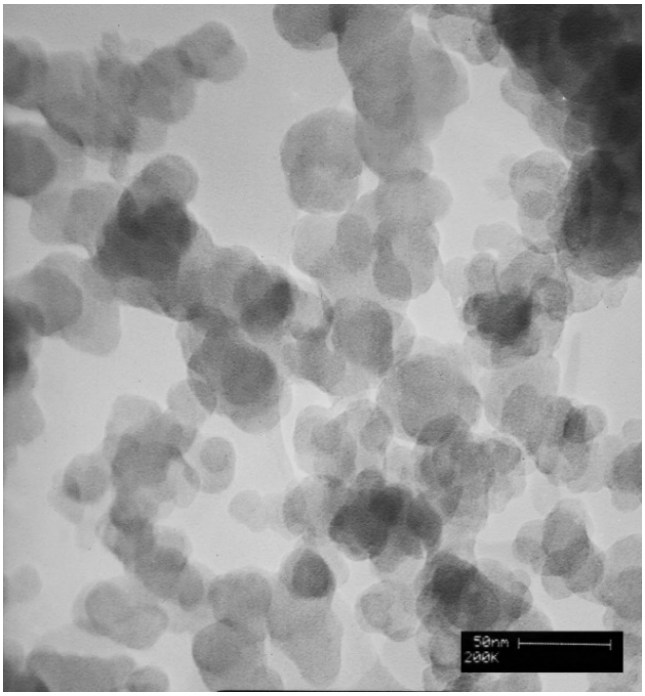

Fig. S5. SEM analysis of nano-Fe_3O_4.

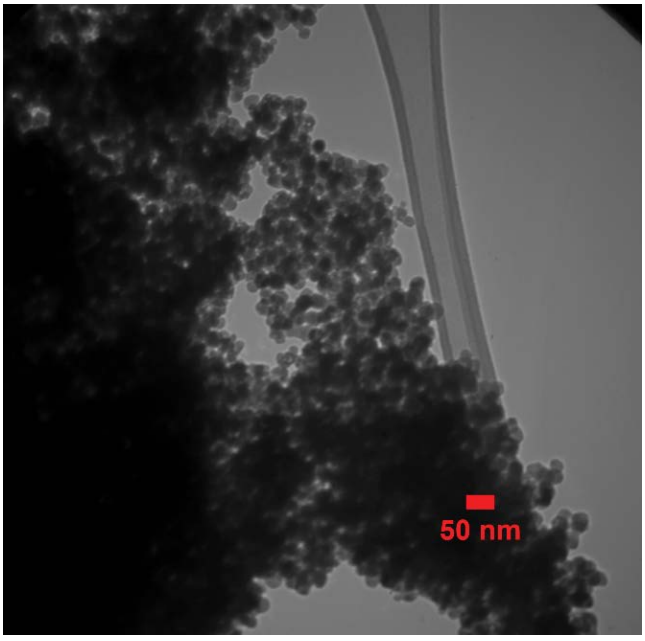

Fig. S6. TEM analysis of nano-Fe_3O_4.